# Counterion Effect on the Morphological and Mechanical Properties of Polymer−Clay Nanocomposites Prepared in an Aqueous Medium

Fábio do Carmo Bragança, Leonardo Fonseca Valadares, Carlos Alberto de Paula Leite, and Fernando Galembeck*

*Institute of Chemistry, Universidade Estadual de Campinas, Caixa Postal 6154, 13084-971, Campinas SP, Brazil*

*Received February 16, 2007. Revised Manuscript Received April 5, 2007*

Na−montmorillonite (Na-MMT) and its ion-exchanged derivatives (K-, Li-, Ca-MMT) were used to make nanocomposites by mixing with a low-$T_g$ styrene−acrylic latex, and these materials were used to verify the effects of counterions on nanocomposite morphology and mechanical properties. The monovalent cation clays form exfoliated/intercalated nanocomposites with a more than 10-fold increase in modulus, as compared to the pristine polymer, and approximately 200% increase in tensile strength. In the case of Li nanocomposites the mechanical properties are strongly dependent on the extent of drying, as expected considering that these ions are strongly hydrated. Calcium clay−polymer particle adhesion is very good, as evidenced in transmission electron micrographs, but the extent of exfoliation is less pronounced and the changes in the mechanical properties are accordingly lower than using Na, Li, or K counterions. Analytical electron micrographs show that the counterions are always accumulated in the domains containing both clay and polymer, showing that the compatibility of these two phases, which carry excess negative charges, is achieved thanks to cation bridges at the interfaces, following a model that was previously put forward to explain latex−clay nanocomposite formation and properties.

## Introduction

Nanocomposite[1−3] materials made by dispersing layered silicates (clays) within polymers or rubbers are interesting because they can be designed to display often-required combinations of mechanical, thermal, permeation, and optical properties[4−6] as well as chemical and swelling resistance to oil and solvents.[7] This is due to the peculiar properties of clay and polymers used and also to the micromorphologies that are achieved and are responsible for, for example, anisotropy introduced into the material by exfoliated or intercalated clay.[8]

One of the most intensively studied layered silicates for nano-reinforcement is montmorillonite because of its high surface area and reactivity,[9] coupled to the large aspect ratio of individual lamellar particles[10] and significant ion-exchange capacity within aqueous media.[11] Its basic structure consists of lamellae formed by two tetrahedral silicate sheets on both sides of an octahedral aluminate sheet. Isomorphous substitution ($Al^{3+}$ for $Si^{4+}$ in tetrahedral sheets or $Mg^{2+}$ or $Fe^{2+}$ for $Al^{3+}$ in octahedral sheets) within the layers generates negative charges that are counterbalanced by cations (typically $Na^+$ or $Ca^{2+}$ in natural montmorillonites). The stacking of the layers leads to a regular van der Waals gap between them, called the interlayer or gallery.[12]

In aqueous media, the water molecules can penetrate the interlayer space, reducing the attractive forces between the layers and the counterions, leading to lamellae separation on the order of tens of nanometers with a high aspect ratio and plate-like structure.[13,14]

In polymer−clay nanocomposites, the separation of the lamellae and the adhesion of these lamellae at the polymer matrix play a crucial role in the properties of these systems. These two characteristics are concurrent, because polymer−platelet adhesion is required for keeping lamellae well-separated.

The use of aqueous colloidal polymer dispersions (latex) to introduce the polymer phase in the nanocomposite preparation facilitates lamellae separation, and it is the basis of a useful methodology to make cross-linked polymer/clay nanocomposites.[15,16] In a previous work from this laboratory,[8] we examined the properties and the formation mechanism of non-vulcanized natural rubber nanocomposites prepared

* To whom correspondence should be addressed. E-mail: fernagal@iqm.unicamp.br. Phone: +55-19-3521-3080. Fax: +55-19-3521-2906.

(1) Varghese, S.; Karger-Kocsis, J. *Polymer* **2003**, *44*, 4921.
(2) Wheeler, P. A.; Wang, J.; Mathias, L. J. *Chem. Mater.* **2006**, *18*, 3937.
(3) Karger-Kocsis, J.; Wu, C. M. *Polym. Eng. Sci.* **2004**, *44*, 1083.
(4) Haraguchi, K.; Ebato, M.; Takehisa, T. *Adv. Mater.* (Weinheim, Germany) **2006**, *18*, 2250.
(5) Wang, Z.; Pinnavaia, T. J. *Chem. Mater.* **1998**, *10*, 3769.
(6) Manaias, E.; Touny, A.; Wu, L.; Strawhecker, K.; Lu, B.; Chung, T. C. *Chem. Mater.* **2001**, *13*, 3516.
(7) Takeichi, T.; Guo, Y. *J. Appl. Polym. Sci.* **2003**, *90*, 4075.
(8) Valadares, L. F.; Leite, C. A. P.; Galembeck, F. *Polymer* **2006**, *47*, 672.
(9) Ray, S. S.; Okamoto, M. *Prog. Polym. Sci.* **2003**, *28*, 1539.
(10) Ammann, L.; Bergaya. F.; Lagaly, G. *Clay Miner.* **2005**, *40*, 441.
(11) Lagaly, G.; Ziesmer, S. *Adv. Colloid Interface Sci.* **2003**, *100*, 105.
(12) Hussain, F.; Okamoto, M.; Gorga, R. E. *J. Compos. Mater.* **2006**, *40*, 1511.
(13) Lin, J.-J.; Chu, C.-C.; Chiang, M.-L.; Tsai, W.-C. *J. Phys. Chem. B* **2006**, *110*, 18115.
(14) Wu, Y. P.; Wang, Y. Q.; Zhang, H. F. *Compos. Sci. Technol.* **2005**, *65*, 1195.
(15) Wu, Y. P.; Zhang, L. Q.; Wang, Y. Q.; Liang, Y.; Yu, D. S. *J. Appl. Polym. Sci.* **2001**, *82*, 2842.
(16) Hwang, W. G.; Wei, K. H.; Wu, C. M. *Polymer* **2004**, *45*, 5729.

10.1021/cm070467+ CCC: $37.00 
Published on Web 05/27/2007

**Table 1. Cation Concentration in the Pristine and Ion-Exchanged Clays Determined by ICP-OES**

| | sodium (mequiv/ 100 g) | calcium (mequiv/ 100 g) | lithium (mequiv/ 100 g) | potassium (mequiv/ 100 g) |
|---|---|---|---|---|
| Ca-MMT | 1.3 | 89.8 | *a* | *a* |
| Li-MMT | 17.0 | 0.9 | 58.0 | *a* |
| K-MMT | 3.8 | *a* | *a* | 71.6 |
| Na-MMT | 117.3 | 1.9 | *a* | *a* |

[a] Below detection limit.

**Table 2. Mechanical Properties of Styrene−Acrylic Latex and Ion-Exchanged Clay Nanocomposites**

| | tensile strength (MPa) | Young's modulus (MPa) | max strain (%) |
|---|---|---|---|
| styrene−acrylic | 2.4 ± 0.2 | 34 ± 12 | 542 ± 53 |
| styrene−acrylic + Ca-MMT | 3.8 ± 0.2 | 171 ± 29 | 305 ± 38 |
| styrene−acrylic + Li-MMT | 4.6 ± 0.6 | 316 ± 30 | 151 ± 34 |
| styrene−acrylic + K-MMT | 6.9 ± 0.6 | 411 ± 33 | 77 ± 19 |
| styrene−acrylic + Na-MMT | 7.1 ± 0.5 | 375 ± 39 | 59 ± 23 |

using latex. This method allows the formation of nanocomposite materials, irrespective of the previous surface modification or hydrophobicization of the clay. This can be understood considering the electrostatic charge patterns within the colloidal dispersion, where particles with a given charge are dispersed in a solution with opposite charge excess, due to counterions. Upon drying, polymer/clay particles are strongly attracted by ionic interactions and van der Waals forces, bonding the different phases. Following this model, the properties of nanocomposites made by drying mixed clay−polymer aqueous dispersions should be dependent mainly on the counterions found in the dispersion.

In this study, we describe the effects of the different interlayer cations on some properties and morphology of the rubber−clay nanocomposites, obtained using the latex−clay dispersion method. Potassium, lithium, and calcium homoionic clays were carefully prepared, and the effects of these ions on the properties of poly(styrene-*co*-butyl acrylate-*co*-acrylic acid)/clay nanocomposite at a 10 phr clay were determined and compared to the native sodium clay, by using stress−strain analysis, X-ray diffraction (XRD), X-ray microtomography, and analytical transmission electron microscopy based on electron energy loss spectroscopy imaging (ESI-TEM).

## Experimental Section

**Latex Synthesis.** The poly(styrene-*co*-butyl acrylate-*co*-acrylic acid) latex (styrene−acrylic latex) was prepared by emulsion polymerization in a kettle glass reactor using two magnetic drive gear pumps (Cole Parmer model 7144-02) for adding the redox initiator (4.3 g of sodium persulfate from Synth dissolved in 85 mL of water) and an emulsion containing monomers, water, and surfactant.

The monomer emulsion was prepared by dissolving 19 g of the surfactant (Renex 40 that is ethoxylated nonylphenol with four ethylene oxide units, Oxiteno) in 280 mL of deionized water followed by monomer addition [266.0 g of styrene (CBE), 306.5 g of butyl acrylate (BASF), and 11.5 g of acrylic acid (BASF)] and stirring using a Cowles disperser at 2000 rpm for 10 min. The monomer emulsion and the redox initiator were added simultaneously during 4 and 4.5 h, respectively.

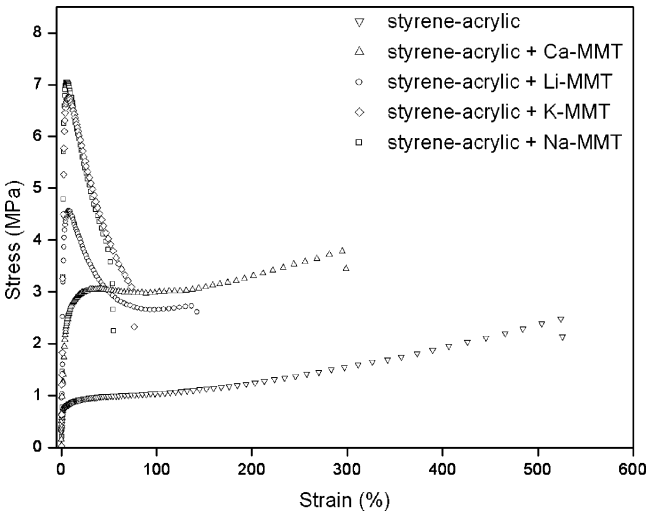


**Figure 1.** Stress vs strain curves for styrene−acrylic latex (s-a) and ion-exchanged clay nanocomposites.

The temperature was kept at 60−65 °C. After completing the reactant addition, the temperature was kept for 1 h to decrease residual monomers content. The reaction was finalized with 15 mL of a *tert*-butyl hydroperoxide solution (14 wt %). The final dispersion was cooled to room temperature and filtered through a 90 $\mu$m polyamide screen, when a small amount of coagulated latex (4.5 g) was collected. The pH was adjusted to 7.0 by using 100 mL of an ammonium hydroxide aqueous solution (20%, v/v). Effective latex particle diameter and zeta potential determined by PCS in a Brookhaven Zeta Plus instrument are respectively 950 nm and −29 mV.

**Preparation of K−, Li−, and Ca−Montmorillonites.** Sodium montmorillonite (Na-MMT) was acquired from Southern Clay Products (cation exchange capacity = 102 mequiv/100 g of clay) and used as received.

K-, Li-, and Ca-MMTs were prepared by exchanging Na for the corresponding cations. The procedure consists in dispersing 50 g of sodium montmorillonite in 10 L of deionized water, under stirring at 70 °C. After 60 min, 25 g of LiCl (Acros) or KCl (Merck) or 35 g of $CaCl_2$ (Merck) was added to the suspension. The dispersions were kept stirring for 24 h at 70 °C. The excess salt was then removed by dialysis, using regenerated cellulose dialysis bags immersed in deionized water that was daily exchanged until the conductivity of the external water was less than 2 $\mu$S (20 days).

**Clay Elemental Analysis.** A dry sample of each clay (Na-, K-, Li-, and Ca-MMT) was manually ground in a mortar and passed through a 150 $\mu$m opening sieve. These samples were then dried in an oven at 100 °C for 8 h and kept in a desiccator. For the elemental analysis, 100 ± 0.1 mg of each clay was weighed in a polypropylene beaker, followed by addition of 2.0 mL of HF (48 wt % Vetec) and 1 mL of $HNO_3$ (65 wt % Merck). After 8 h, 0.25 mL of $H_2SO_4$ (50%, v/v, Merck) and 1 mL of HF were added, and the dispersion was heated to dryness. The solids were dissolved with 1 mL (50%, v/v, Merck) of HCl, 1 mL of $HNO_3$, and 100 mL of deionized water. The resulting clear solution was analyzed by ICP-OES (Perkin-Elmer, Optima 3000-DV), using instrumental conditions adequate for aqueous solutions (plasma power, 1.3 kW; nebulization flow rate, 0.8 L·min$^{-1}$).[17]

**Preparation of Nanocomposites.** The ion exchange procedure yielded clay dispersions with 5 wt % solids content. To prepare

(17) Boss, C. B.; Fredeen, K. J. *Concepts Intrumentation and Techniques in Inductively Coupled Plasma Optical Emission Spectrometry*, 2nd ed.; Perkin-Elmer Corp.: Norwalk, 1999.

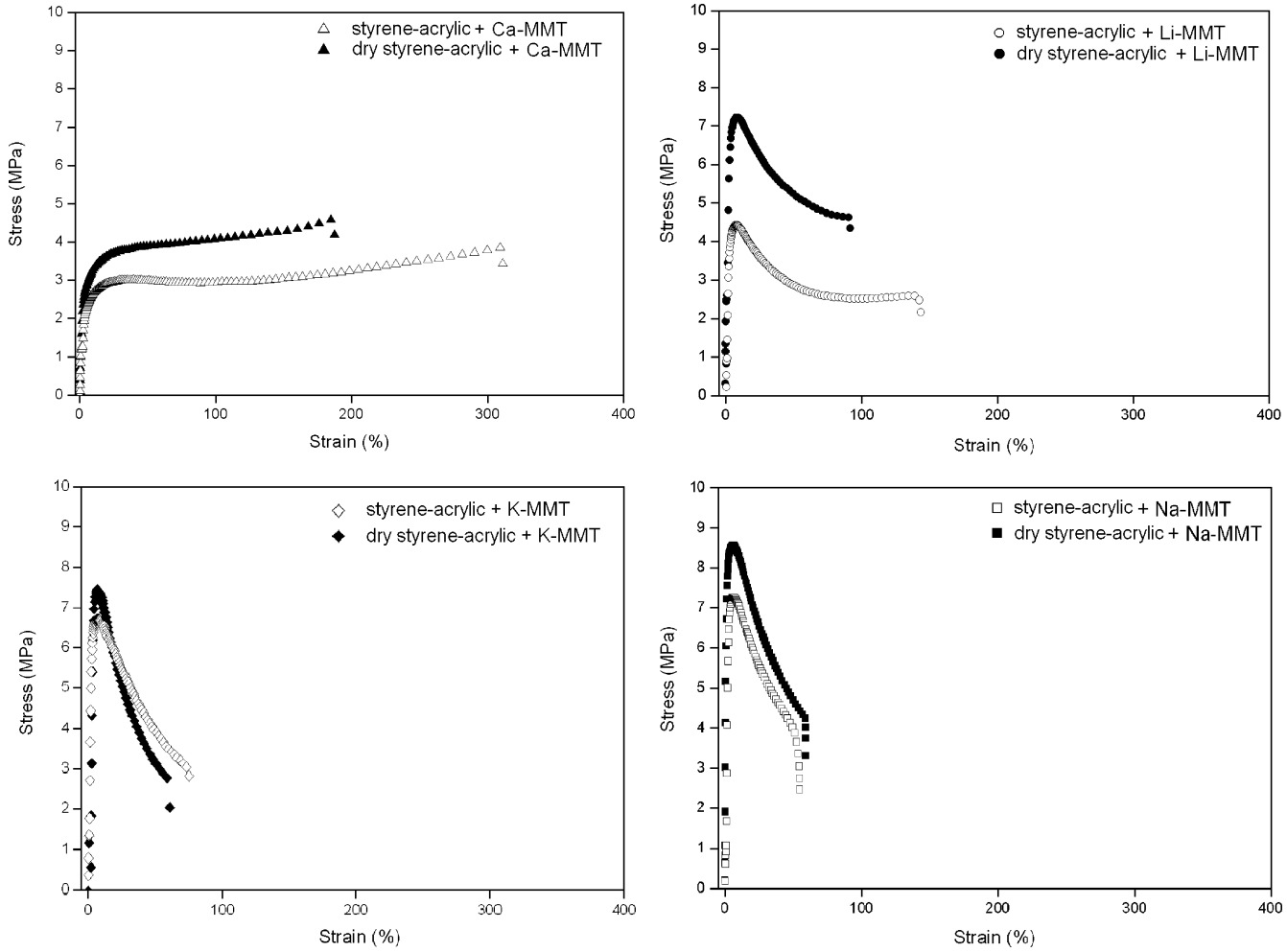


**Figure 2.** Stress vs strain curves for styrene−acrylic latex and ion-exchanged clay nanocomposites dried at 120 °C for 72 h.

**Table 3. Mechanical Properties of Ion-Exchanged Clay Nanocomposites Extensively Dried**[a]

| | tensile strength (MPa) | Young's modulus (MPa) | max strain (%) |
|---|---|---|---|
| styrene−acrylic + Ca-MMT | 4.6 ± 0.2 | 177 ± 23 | 180 ± 21 |
| styrene−acrylic + Li-MMT | 7.4 ± 0.3 | 492 ± 50 | 98 ± 26 |
| styrene−acrylic + K-MMT | 7.5 ± 0.7 | 458 ± 54 | 61 ± 12 |
| styrene−acrylic + Na-MMT | 8.8 ± 0.6 | 473 ± 52 | 60 ± 14 |

[a] Bare styrene−acrylic polymer cannot be tested because the sample is fluid at 120 °C, while the nanocomposite samples are not deformed.

the nanocomposites, 19.7 g of latex (46.2 wt %) were mixed with 18 g of the respective clay dispersion (K-, Li-, or Ca-MMT) with a magnetic stirrer during 30 min.

To prepare the Na-MMT/latex nanocomposite, 0.9 g of the as-received montmorillonite were dispersed in 180 mL of deionized water and left equilibrating for 20 days. After this period, the clay dispersion was mixed to 19.7 g of latex under the same conditions of the other systems. The mixed clay−latex dispersions were thick slurries, and they were transformed into monoliths by casting on flat plastic molds (10 × 10 × 0.2 cm) that were dried in an oven under air at 60 °C for 24 h.

**Instruments and Measuring Procedures.** Tensile tests were performed according to DIN 52504 standard using specimens cut from the samples prepared by casting (2 ± 0.2 mm) thickness. All specimens were kept at 24 °C under a 50% relative humidity for 24 h before the measurements were performed using an EMIC DL2000 universal testing machine at a strain rate of 200 mm/min. Ten specimens were tested for each sample and the reported values are the calculated averages. The Young modulus[18] was obtained from the angular coefficient in the initial linear portion ($\epsilon < 0.5\%$) of the stress−strain plots.

Wide-angle X-ray diffraction (WAXD) measurements were performed using a Shimadzu XRD-7000 diffractometer in the reflection mode with an incident Cu Kα radiation, 1.54 Å wavelength, under 0.5°/min scan rate. Stratified clay samples were prepared by drying 10 mL of a 5 wt % dispersion within a Teflon tray. This was placed within an oven at 120 °C, and bulk water evaporation was observed during the first 3 h, but the sample was kept within the oven for 48 h. For the nanocomposite, dry cast films were laid on the sample holder for WAXD measurements. Both film sides were examined.

The X-ray microtomograph equipment used is a desktop X-ray micro-CT scanner (SkyScan 1074, Aartselaar, Belgium), equipped with a 768 × 576 pixels 8-bit X-ray camera in on-chip integration mode with the lens coupled to a scintillator (30 μm of resolution). As a reference, a film cast from poly(styrene−acrylic) latex was layered over each nanocomposite film, prior to imaging.

For TEM analysis, ultrathin (ca. 50 nm) sections were cut normal to the nanocomposite film plane, using a diamond knife (Drukker) in a Leica EM FC6 cryo-ultramicrotome cooled with liquid $N_2$ at −140 °C. A Carl Zeiss CEM 902 (80 kV) transmission electron microscope fitted with a Castaing-Henry energy filter spectrometer was used to examine the cuts. Elemental images were obtained for the relevant elements found in the sample using the three-window

(18) Hunt, B. J.; James, M. I. *Polymer Characterisation*; Chapman and Hall: London, 1997.

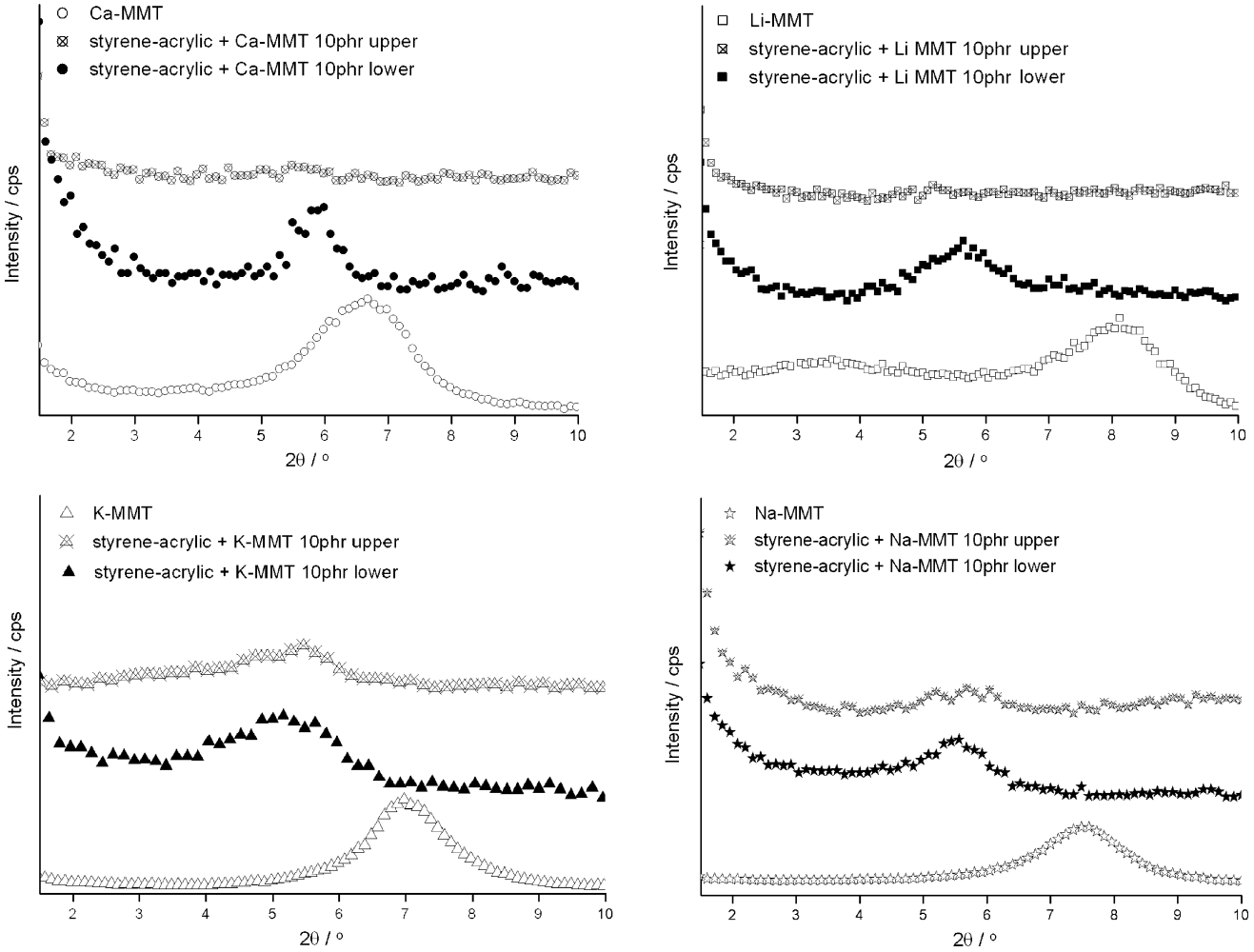


**Figure 3.** WAXD for ion-exchanged clays and respective poly(styrene−acrylic) nanocomposites. Upper panels, dried in contact with air; lower panels, dried in contact with the plastic mold surface.

method and the carbon K-edge, silicon L-edge, and calcium L-edge. The energy-selecting slit was set at 303 eV for C, 132 eV for Si, and 352 eV for Ca with a 15 eV slit width.[19] The images were acquired using a slow scan CCD camera (Proscan) and processed in the iTEM Universal Imaging Platform.

## Results

Extensive sodium ion exchange by $K^+$, $Li^+$, and $Ca^{2+}$ ions was obtained using the procedure described in this work, and the exchangeable ion concentrations in the clays are given in Table 1. $Ca^{2+}$, $Li^+$, $K^+$, and $Na^+$ ions are each prevalent in one of the four samples, for which reason these are named Ca-MMT, Li-MMT, K-MMT, and Na-MMT, respectively.

Clay−polymer nanocomposites mechanical behavior under stress varies widely depending on the counterion, as shown in Table 2 and Figure 1: the bare polymer test samples have a low modulus and are easily strained above 500% under less than 2 MPa stress, showing the typical behavior of a low-$T_g$ polymer. The nanocomposites with Na-MMT and K-MMT have large initial moduli, respectively 375 and 411 MPa, and they start to form necks under stresses in the 7−8 MPa range, showing an overall behavior that resembles that of semicrystalline thermoplastics, for example, low-density polyethylene. Styrene−acrylic/Ca-MMT nanocomposite necks under 4 MPa stress only, but it can be strained to >300% before rupture. These results verify the initial hypothesis from this work: in latex/clay nanocomposites the ion species in the clay has a major effect on the nanocomposite mechanical behavior, thus supporting the following model: clay lamellae and the polymer matrix are tightly bonded, mediated by counterions.

The importance of counterion effect on the nanocomposite mechanical properties is further verified by observing the effect of extensive drying of the nanocomposites (120 °C for 120 h) on their stress−strain curves, as shown in Table 3 and Figure 2. In every case the limiting stress for polymer necking increases by at least 10%, and the large maximum strains of the nanocomposites with Ca-MMT and Li-MMT decrease. The largest modulus change in this case is presented by the dry polymer/Li-MMT nanocomposite, with an approximately 60% increase over the modulus reported in Table 2 for the as-prepared Li-MMT. This difference can be assigned to dehydration of the $Li^+$ counterions and also of the anionic sites responsible for electrostatic adhesion at the clay−polymer interfaces, causing a decrease in the

(19) Reimer, L., Zepke, U. J., St. Schulze-Hillert, M., Ross-Messemer, M., Probst, W., Weimer, E., Eds.; *EELS Spectroscopy: A Reference Handbook of Standard Data for Identification and Interpretation of Electron Energy Loss Spectra and for Generation of Electron Spectroscopic Images*; Carl Zeiss: Oberkochen, 1992.

**Table 4. Interlayer Distance of Ion-Exchanged Clay**

| system | clay $d_{(001)}$ (Å) | clay $d_{(001)}$ − 9.6[a] (Å) | ion radius[b] × 2 (Å) | clay $d_{(001)}$ (Å) (literature) | refs |
|---|---|---|---|---|---|
| Ca-MMT | 13.3 | 3.7 | 1.9 | 11.19−12.45 | 21−24 |
| Li-MMT | 10.9 | 1.3 | 1.2 | 10.11−12.5 | 25−27 |
| K-MMT | 12.2 | 2.6 | 2.6 | 10.9−12.5 | 28−31 |
| Na-MMT | 11.7 | 2.1 | 1.9 | 11.0−12.8 | 32−35 |

[a] Reference 36. [b] Reference 37.

**Table 5. Interlayer Distance in Ion-Exchanged Clay Nanocomposites and Gallery Dimensions**

| system | initial opening (clay $d_{(001)}$ − 9.6 Å) | nanocomposite $d_{(001)}$ dried at 60 °C | nanocomposit $d_{(001)}$ dried at 120 °C | nanocomposite gallery ($d_{(001)}$ − 9.6 Å) |
|---|---|---|---|---|
| Ca-MMT | 3.7 | 14.7 | 15.0 | 5.4 |
| Li-MMT | 1.3 | 15.7 | 15.1 | 5.5 |
| K-MMT | 2.6 | 16.7 | 15.0 | 5.6 |
| Na-MMT | 2.1 | 16.0 | 15.2 | 5.6 |

interionic distances and consequently an increase in the interionic forces.

X-ray diffractograms are given in Figure 3. Na-, Li-, and K-MMT, the interlayer openings given in Table 4, are in agreement with the known ion diameters. However, the spacing for Ca-MMT clay is significantly larger than the anhydrous calcium ion diameter. A possible explanation for this difference is $Ca^{2+}$ ion residual hydration and perhaps also $Ca^{2+}$ ion partial hydrolysis, both due to its higher charge. Beyond hydration, Bray et al.[20] have also considered the possibility of $Ca^{2+}$ irregular distribution in the gallery.

WAXD results for styrene−acrylic clay nanocomposites are given in Table 5 and Figure 3. As the samples were prepared by casting, great attention was given to the differences between the upper face, formed in contact with air, and the lower face, formed in contact with the mold surface. The values shown in Table 5 refer to the latter for all polymer/clay nanocomposites. In Figure 3, accordance with the Table 5 characteristic diffraction peak $d_{(001)}$ for the extensively dried nanocomposites appears shifted to a low-angle region: 1.7 Å for the styrene−acrylic/Ca-MMT, 4.2 Å for the styrene−acrylic/Li-MMT, 2.8 Å for the styrene−acrylic/K-MMT, and 3.5 Å for styrene−acrylic/Na-MMT nanocomposites as compared to the respective clay, evidencing the formation of intercalated nanocomposites. The smaller initial opening (clay $d_{(001)}$ − 9.6 Å) leads to the larger interlayer expansion (nanocomposites $d_{(001)}$ − clay $d_{(001)}$ Å),

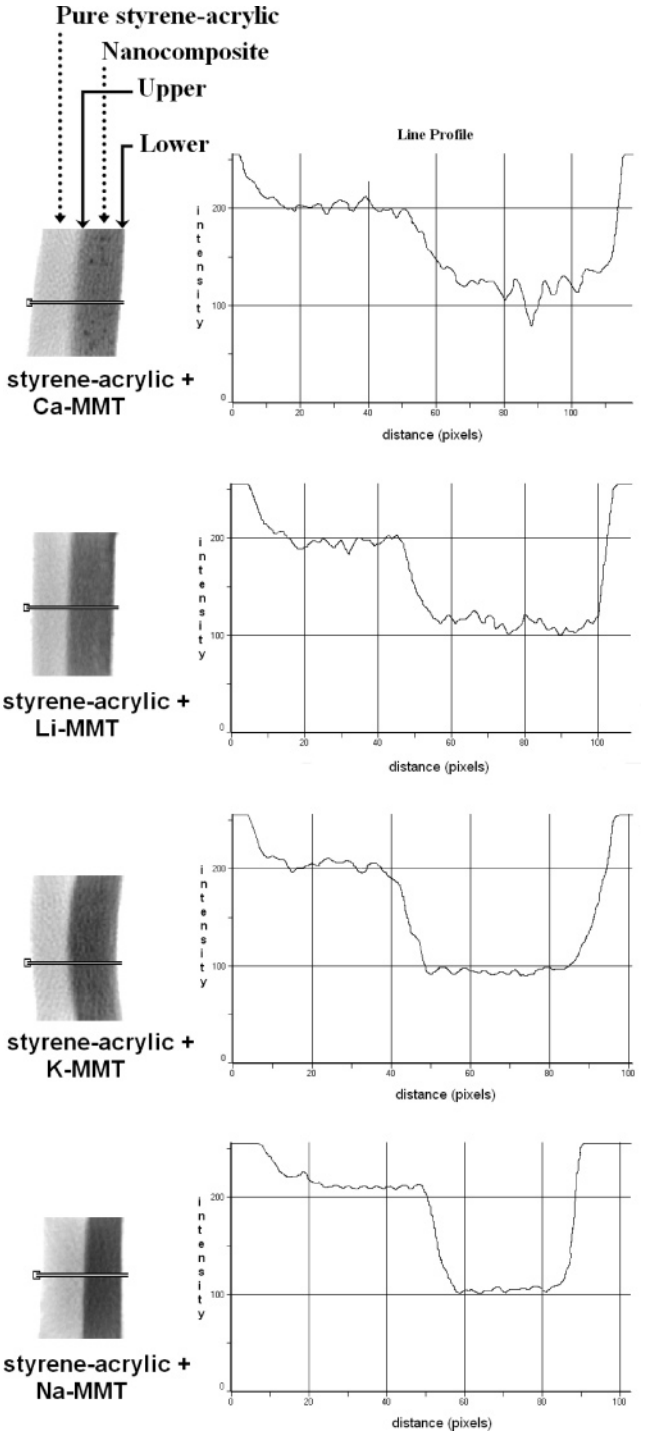


**Figure 4.** X-ray microtomographs of styrene−acrylic polymer and ion-exchanged clay nanocomposites.

(20) Bray, H. J.; Redfern, S. A. T.; Clark, S. M. *Mineral. Mag.* **1998**, *62*, 647.
(21) Sato, T.; Watanabe, T.; Osuka, R. *Clays Clay Miner.* **1992**, *40*, 103.
(22) Pezerat, H.; Mering, J. *C. R. Acad. Sci.* (Paris) **1967**, *265*, 529.
(23) Bray, H. J.; Redfern, S. A. T.; Clark, S. M. *Mineral. Mag.* **1998**, *62*, 647.
(24) Cases, M.; Berend, I.; François, M.; Uriot, J. P.; Michot, L. J.; Thomas, F. *Clays Clay Miner.* **1997**, *45*, 8.
(25) Quirk, J. P.; Marcelja, S. *Langmuir* **1997**, *13*, 6241.
(26) Ferrage, E.; Lanson, B.; Sakharov, B. A.; Drits, V. A. *Am. Mineral.* **2005**, *90*, 1358.
(27) Boek, E. S.; Coveney, P. V.; Skipper, N. T. *J. Am. Chem. Soc.* **1995**, *117*, 12608.
(28) Denis, J. H.; Keall, M. J.; Hall, P. L.; Meeten, G. H. *Clay Miner.* **1991**, *26*, 255.
(29) Hendricks, S. B.; Nelson, R. A.; Alexander, L. T. *J. Am. Chem. Soc.* **1940**, *62*, 1457.
(30) Sinegani, A. A. S.; Emtiazi, G.; Shariatmadari, H. *J. Colloid Interface Sci.* **2005**, *290*, 39.
(31) de Chavez, M.; de Pablo, L.; de Pablo, J. J. *Langmuir* **2004**, *20*, 10764.
(32) Cases, J. M.; Berend, I.; Besson, G.; Francois, M.; Uriot, J. P.; Thomas, F.; Poirier, J. E. *Langmuir* **1992**, *8*, 2730.
(33) Moore, D. M.; Reynolds, R. C. *X-Ray Diffraction and the Identification Analysis of Clay Minerals*, 2nd ed.; Oxford University Press: New York, 1997.
(34) Bongiovanni, R.; Mazza, D.; Ronchetti, S.; Turcato, E. A. *J. Colloid Interface Sci.* **2006**, *296*, 515.
(35) Chang, F. R. C.; Skipper, N. T.; Sposito, G. *J. Am. Chem. Soc.* **1995**, *11*, 2734.
(36) Lagaly, G. *Clay Miner.* **1970**, *16*, 1.
(37) Yizhak, M. *Ion Solvation*, 1st ed.; John Wiley & Sons, Inc.: New York, 1985.

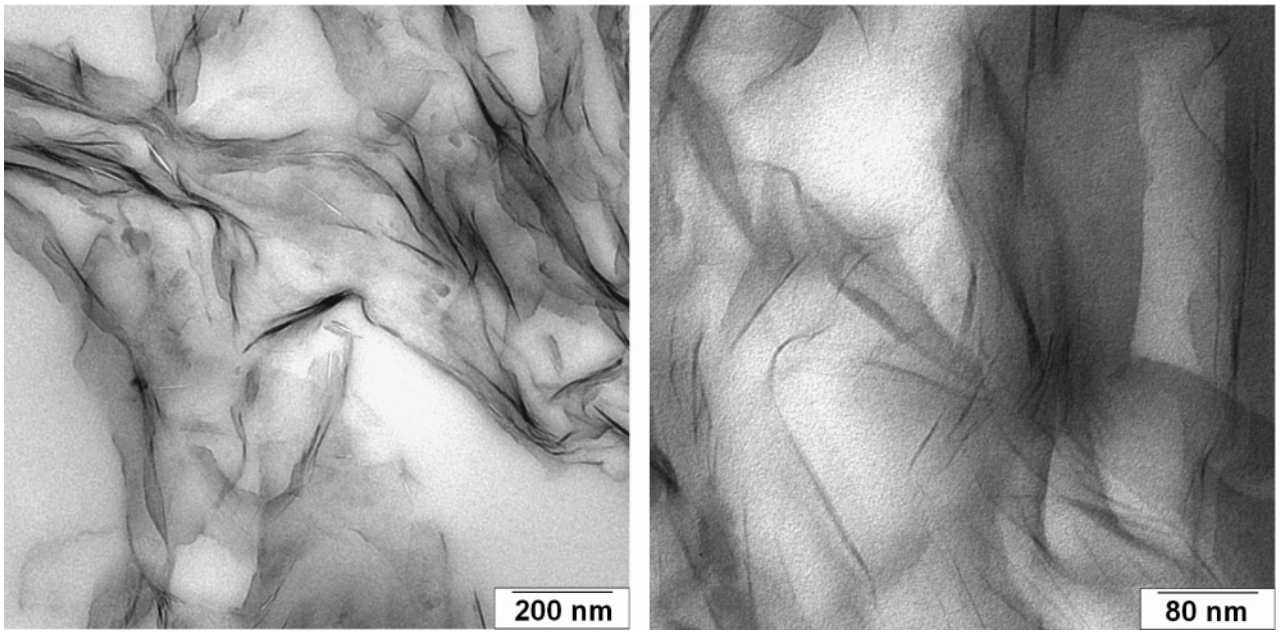


**Figure 5.** TEM micrographs of 10 phr Na-MMT styrene−acrylic nanocomposite. The thin cuts were made normal to the nanocomposite film plane.

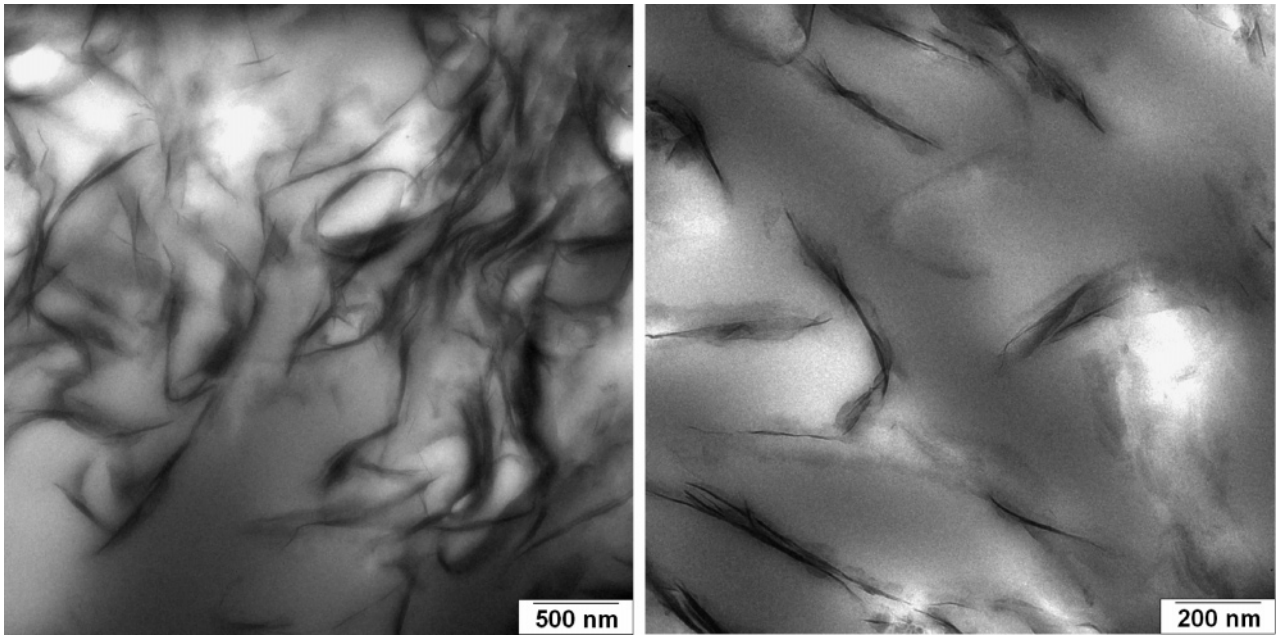


**Figure 6.** TEM micrographs of 10 phr Ca-MMT styrene−acrylic nanocomposite. The thin cuts were made normal to the nanocomposite film plane.

but the same gallery opening is observed for all nanocomposites (5.4−5.6 Å).

X-ray microtomography analysis was used to verify sample homogeneity. To do this, the upper surface of the nanocomposite films was joined to a pure latex film, used as a reference. Figure 4 shows tomography slice images together with linescan plots of gray-level intensity measured along the stripes. The Ca-MMT nanocomposite presents a gradual gray-level variation in the border between pure latex and nanocomposite bulk. The line-profile analyses of the other systems show a sharper variation as compared to the Ca-MMT. Thus, the upper face of the Ca nanocomposite is depleted in Ca, probably as a result of the sedimentation of Ca-MMT during film drying.

For TEM analysis, the center of the films (∼1 mm) was cut and examined. The polymer/Na-MMT nanocomposite cuts (Figure 5) show exfoliated clay lamellae together with some very small tactoids, while exfoliated lamellae are seldom observed in the Ca-MMT nanocomposite images shown in Figure 6. Even so, polymer−clay particle compatibility is very good in Ca-MMT nanocomposite, evidenced by the integrity of the clay−polymer interfaces that is clearly observed without any hole or ruptured film area. Moreover, the Ca map in Figure 7 shows that these ions are always superimposed to clay particles, as expected considering that the cations are sandwiched between clay and polymer negative surfaces.

## Discussion

The results described in this paper verify the following hypothesis: the good affinity between polymer and clay in nanocomposites prepared in aqueous medium allows the

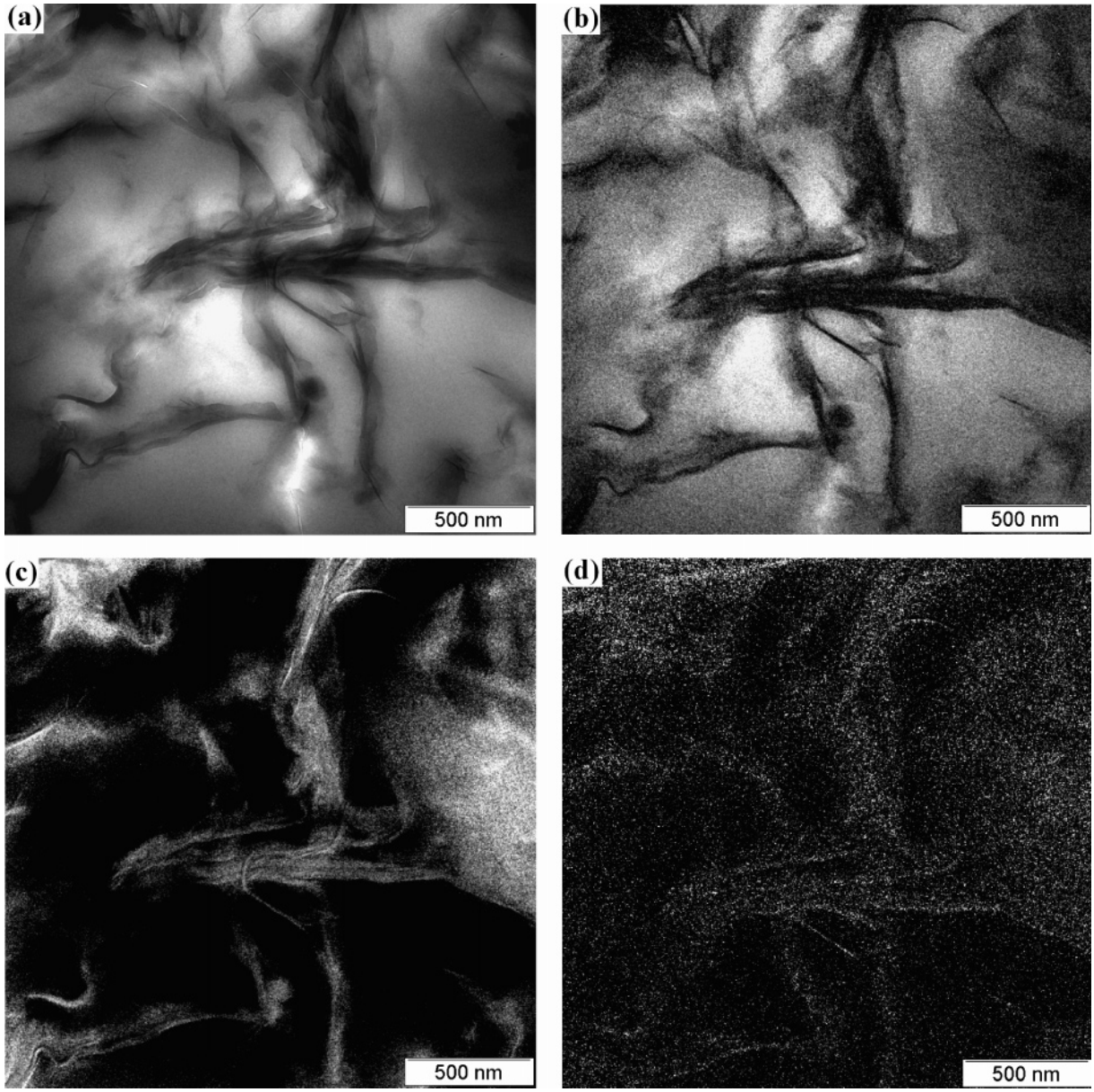


**Figure 7.** ESI-TEM micrographs of 10 phr Ca-MMT styrene−acrylic nanocomposite thin cuts. (a) Bright field image, (b) carbon map, (c) silicon map, and (d) calcium map.

control of their properties just by exchanging the counterions and using the ion-exchanged clays to prepare nanohybrid materials in aqueous medium.

The dependence on the intervening cations is easily understood, considering the model for clay−polymer adhesion schematized in Figure 8. According to this model, positive counterions are responsible for the strong adhesion between the clay and the latex particles that (both) contain excess negative charges but can be rendered compatible thanks to the electrostatic interaction created by the deposition of a layer of positive ions at the interface.

Young's modulus enhancement is dominated by the high aspect ratio of the clay platelets and the interfacial strength.[38] In this work, only the clay counterions were changed, so the difference of the nanocomposite Young's moduli presented in Table 2 is mainly ascribed to the ionic electrostatic forces and clay morphology.

An interesting further confirmation of this model is obtained by observing that the largest effects of nanocomposite drying are obtained in the case of lithium ions. As a result of the large charge/radius ratio of non-solvated $Li^+$ ions, they are strongly hydrated, and the hydrous ions have in turn a much smaller charge/radius ratio than the dry ions.[37,39] Consequently, the electrostatic interactions involving these ions are those changing most when the samples are dried, as evidenced by the tensile strength and modulus that increase by approximately 50% when the polymer/Li-MMT nanocomposite is dried at 120 °C for a 5-day period.

Okamoto et al.[40,41] observed that a smaller initial opening in a modified clay leads to the larger interlayer expansion

(38) Rao, Y. Q.; Pochan, J. M. *Macromolecules* **2007**, *40*, 290.
(39) Kolthoff, I. M. *Treatise on Analytical Chemistry*, 2nd ed.; John Wiley & Sons Inc.: New York, 1982.
(40) Yoshida, O.; Okamoto, M. *J. Polym. Eng.* **2006**, *26*, 919.
(41) Saito, T.; Okamoto, M.; Hiroi, R.; Yamamoto, M.; Shiroi, T. *Macromol. Mater. Eng.* **2006**, *291*, 1367.

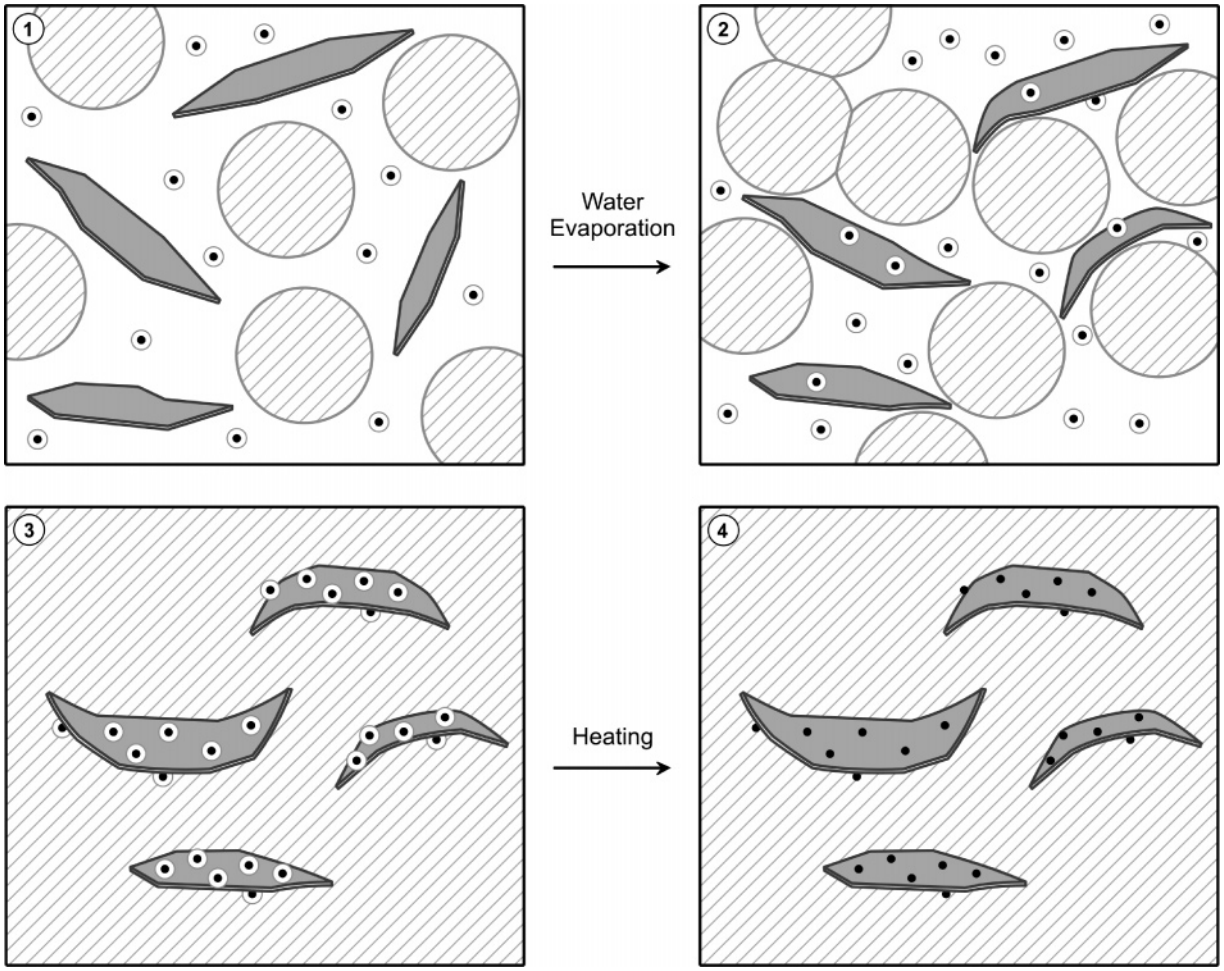


**Figure 8.** Schematic representation of the role of positive counterions (small circles) on the adhesion between clay lamellae and polymer. (1) Latex and clay dispersion, (2) polymer−clay particles approach during dispersion drying, (3) hydrated counterions bridging clay and the dry polymer matrix, and (4) dehydrated counterions bridge clay lamellae and the polymer matrix.

in nanocomposites prepared using different organo-clays, and this was assigned to the balance between polymer penetration and stable gallery height controlled by ionic interaction between cation and negative layer charges. In the present case, the nearly constant gallery spacing can be assigned to a uniform conformation of polymer in between the silicate surfaces. This can be understood considering that the styrene−acrylic copolymer is very flexible, the methylene chains are in a trans conformation, and the aromatic ring also lays roughly parallel to the lamellae, while the small cations are interspersed with the polymer. Using an argument from ref 40, this shows that electrostatic attraction between silicate lamellae and gallery cations is sufficiently strong to force polymer chains into a flattened conformation.

To understand the meaning of the total opening in the WAXD analysis it is necessary to understand the mechanism of nanocomposite formation in aqueous medium. When a liquid wets two parallel surfaces, a force **F** acts among these surfaces, and this is a function of the liquid surface tension and the distance between them. This force, given by the Young−Laplace equation,[42] produces capillary adhesion, and it increases during drying, because the liquid meniscus radius decreases. In the dry nanocomposite, polymer chains interact with the large clay surface and cations by electrostatic interactions and H-bonds,[43] forcing the confined polymer into a flat conformation so that the gallery opening is much lower than the polymer gyration radius or particle diameter.

Clay−polymer interfacial adhesion is significant even in the case of the calcium montmorillonite, when clay exfoliation is little pronounced, as observed in the micrographs. The corresponding elemental C and Si maps show that the polymer and clay domains are well connected without any evidence for lack of adhesion, even in the thin microtome cuts. In this material, the mechanical properties of the nanocomposite are not as drastically different from the bare polymer as in the case of polymer/Na-MMT and K-MMT nanocomposites, which can be assigned to the lower degree of exfoliation of the Ca-MMT within the polymer and to the prevalence of tactoids observed in Figures 6 and 7. This means that calcium ions contribute to clay−polymer adhesion but also, as expected, to the adhesion between clay lamellae. This cannot be generalized to other polymers and clays without further experimental verification, but it is observed in the case of the styrene−acrylic polymer used in this work and at the high montmorillonite contents in the nanocom-

(42) Rabinovich, Y. I.; Esayanur, M. S.; Moudgil, B. M. *Langmuir* **2005**, *21*, 10992.

(43) Gatos, K. G.; Százdi, L.; Pukánszky, B.; Karger-Kocsis, J. *Macromol. Rapid Commun.* **2005**, *26*, 915.

posite (10 phr). On the other hand, these results are a confirmation of the large effects of minor ionic constituents in polymer materials that have been disclosed recently.[44,45]

These results open some interesting possibilities for further work. First, different nanocomposites can be prepared, from the same polymer and clay, just by changing the counterions. Moreover, these materials cover a broad range of mechanical and probably other properties as well. Finally, because the electrostatic adhesion responsible for nanocomposite formation is dependent on the nature of the polymer−particle surface rather than on the nature of bulk polymer, it should be possible to make nanocomposite polymer blends rather easily, by adjusting the polymer−particle surface properties irrespective of the polymer bulk properties, thus offering a new alternative to overcome well-known limitations to the making of compatible polymer blends.

## Conclusion

The positive counterions play an important role in the mechanical and morphological properties of polymer−clay nanocomposites prepared from polymer latexes, adding a new possibility for the making of differentiated materials but using a single clay−polymer pair. This is due to the decisive role of cations in polymer−clay interfacial adhesion, where they form ionic bridges bonding together the two immiscible phases that (both) contain excess negative charges.

**Acknowledgment.** The authors gratefully acknowledge Thiago Gianeti from Unicamp for the clay ICP-OES analysis and the fellowships from CNPq and Capes. This is a contribution from the Millenium Institute for Complex Materials, PADCT/CNPq.

CM070467+

(44) Braga, M.; Costa, C. A. R.; Leite, C. A. P.; Galembeck, F. *J. Phys. Chem. B* **2001**, *105*, 3005.
(45) Rippel, M. M.; Leite, C. A. P.; Galembeck, F. *Anal. Chem.* **2002**, *74*, 2541.